The Astrophysical Journal, 776:103 (9pp), 2013 October 20 doi:10.1088/0004-637X/776/2/103

COSMIC DUST AGGREGATION WITH STOCHASTIC CHARGING

Lorin S. Matthews[1], Babak Shotorban[2], and Truell W. Hyde[1]
[1] Center for Astrophysics, Space Physics, and Engineering Research, Baylor University, Waco, TX 76798, USA; Lorin_Matthews@baylor.edu
[2] Department of Mechanical and Aerospace Engineering, The University of Alabama in Huntsville, Huntsville, AL 35899, USA
Received 2013 March 11; accepted 2013 August 16; published 2013 October 4

ABSTRACT

The coagulation of cosmic dust grains is a fundamental process which takes place in astrophysical environments, such as presolar nebulae and circumstellar and protoplanetary disks. Cosmic dust grains can become charged through interaction with their plasma environment or other processes, and the resultant electrostatic force between dust grains can strongly affect their coagulation rate. Since ions and electrons are collected on the surface of the dust grain at random time intervals, the electrical charge of a dust grain experiences stochastic fluctuations. In this study, a set of stochastic differential equations is developed to model these fluctuations over the surface of an irregularly shaped aggregate. Then, employing the data produced, the influence of the charge fluctuations on the coagulation process and the physical characteristics of the aggregates formed is examined. It is shown that dust with small charges (due to the small size of the dust grains or a tenuous plasma environment) is affected most strongly.

Key words: dust, extinction – interplanetary medium – ISM: general – planets and satellites: formation – plasmas – zodiacal dust

Online-only material: color figures

1. INTRODUCTION

The coagulation of cosmic dust grains is a fundamental process which takes place in astrophysical environments, such as presolar nebulae and circumstellar and protoplanetary disks. Submillimeter observations of T Tauri stars give evidence that as young stellar objects (YSOs) and associated disk material evolve, there is a greater population of large dust grains in the disk, which presumably grow through the agglomeration of smaller grains (Andrews & Williams 2005). The processes by which these aggregates grow to kilometer-sized planetesimals, the precursors to planets, are still poorly understood, though much numerical and experimental work has been done to provide a physical description of the earliest stages of planetesimal formation (see, e.g., Blum & Wurm 2008; Okuzumi 2009; Okuzumi et al. 2011a, 2011b; Matthews et al. 2012 and references therein).

One of the key factors in the growth of aggregate grains is their internal structure. At low velocities, colliding dust particles tend to stick at their point of contact without restructuring (Dominik & Tielens 1997; Dominik et al. 2007), producing fluffy aggregates which are strongly coupled to the ambient gas. Brownian motion, vertical settling, and turbulence are mechanisms which provide a relative velocity of the grains with respect to the gas and to each other, allowing the grains to collide and grow. This growth may continue until the aggregates are up to centimeter sizes, at which point the collision energy is enough to cause compaction (Suyama et al. 2008). One measure of the amount of open space within an aggregate consisting of many spherical monomers is the compactness factor (Paszun & Dominik 2009)

$$\Phi_\sigma = \frac{\sum_{j=1}^{N} a_j^3}{R_\sigma^3}, \quad (1)$$

with N the number of monomers in an aggregate, each with radius a_j, and R_σ the radius of the aggregate's projected cross section averaged over many orientations, referred to as the equivalent radius.

The turbulence within accretion disks is attributed to magnetorotational instability (MRI; Balbus & Hawley 1991). The MRI requires an ionized medium to couple the magnetic field to the disk material. The dust in these ionized regions becomes charged through the collection of electrons and ions, affecting not only the region of turbulence (Sano et al. 2000; Okuzumi 2009) but also the interactions between the grains during the collision process and their resultant morphology (Matthews et al. 2012; Matthews & Hyde 2008; Okuzumi 2009; Okuzumi et al. 2011a, 2011b).

In most cases, grains charge to a negative potential due to greater electron mobility as compared to the ions. Thus, the Coulomb interaction between grains in general is repulsive, inhibiting grain growth, though mechanisms which are capable of producing positively and negatively charged grains trigger runaway growth (Ivlev et al. 2002; Konopka et al. 2005; Matthews & Hyde 2004). However, the coagulation rate for such like-charged grains may be enhanced if charge–dipole interactions, which can be created by anisotropic plasma flow (Lapenta 1998) or induced dipoles (Simpson 1978), are included. The physical geometry of the aggregates can also lead to a net dipole moment on the grain, which has been shown to enhance the coagulation rate for like-charged grains (Matthews & Hyde 2008, 2009).

The effect of the dust charging on aggregate growth depends on the relative densities of the gas and dust. High dust densities lead to electron depletion, and the resultant difference in grain charge has been shown to alter the physical characteristics of the dust aggregates (Matthews et al. 2012). More highly charged dust aggregates tend to be more massive, as they preferentially incorporate the largest monomers from the initial dust population, but also tend to be fluffier, with lower compactness factors and larger equivalent radii. Numerical simulations of the coupling between the dust charge and gas ionization states have shown that porous aggregate growth eventually "freezes out" over a large portion of a protoplanetary disk, halting further dust growth, though this may be prevented by global dust transport (Okuzumi et al. 2011a, 2011b).

Given these effects, a complete understanding of the microphysics underlying the charging and aggregation of dust is still needed. One aspect of dust charging that becomes important in weakly ionized gas environments is the stochastic nature of the charging process as ions and electrons are collected on the surface of the grain at random time intervals. This stochastic behavior is intrinsic noise (Van Kampen 2007), which occurs in systems with discrete nature. Various approaches, based on a time series approach (Cui and Goree 1994), master or Fokker–Planck equations (Matsoukas & Russell 1995, 1997; Shotorban 2011, 2012), and the Langevin equation (Khrapak et al. 1999; Shotorban 2011), have been proposed to model the stochastic charging of spherical dust grains. Shotorban (2011) showed that all of these approaches can be developed from the master equation that governs the state of the grain charge, assuming that the charging is a Markov process.

This study examines how the stochastic charge fluctuations alter the coagulation process and the physical characteristics of the aggregates formed. Section 2 describes the charging model and the manner in which the stochastic fluctuations are taken into account. Section 3 describes the model used to simulate the collisional growth of fractal aggregates and its integration with the charging model. The resultant aggregate morphology is compared for aggregation with stochastic and non-stochastic charging in Section 4, with a summary and conclusion presented in Section 5.

2. CHARGING MODEL

The charge on the surface of an aggregate can be found using orbital motion limited (OML) theory employing a line-of-sight (LOS) approximation, OML_LOS (Matthews et al. 2012). OML theory of cylindrical and spherical Langmuir probes is commonly used to derive the charge on a single grain immersed in plasma (Laframboise & Parker 1973; Whipple 1981). The current density due to incoming ions or electrons (plasma species s, i.e., ions or electrons) to a point on the surface of a grain is given by

$$J_s = q_s n_s \left(\frac{m_s}{2\pi k T_s}\right)^{3/2} \exp\left(-\frac{q_s \Phi}{k T_s}\right) \times \int_{v_{\min}}^{\infty} v_s^3 \exp\left(-\frac{m_s v_s^2}{2 k T_s}\right) dv_s \iint \cos\alpha \, d\Omega, \quad (2)$$

with n_s the plasma density of species s very far from the grain, q_s the charge of the incoming plasma particle of mass m_s and temperature T_s, v_s the velocity of the incoming plasma particle, α the angle between the velocity vector and the surface normal, and Ω the solid angle. The lower limit of integration for the particle velocity is $v_{\min} = \sqrt{-2 q_s \Phi / m_s}$ for $q_s \Phi < 0$ and 0 for $q_s \Phi > 0$, where Φ is the electric potential at the surface of the dust grain.

A critical point in OML theory is that all positive energy orbits connect back to infinity and do not originate from another point on the grain (Laframboise & Parker 1973). In calculating the current density to a spherical grain, plasma particles are allowed to impinge upon any given point on the grain surface from all directions except for those blocked by the grain itself; thus, the limits for angular integration are $0 \leqslant \theta \leqslant \pi/2$ and $0 \leqslant \phi \leqslant 2\pi$, providing an analytical solution for the current density. For an irregular aggregate consisting of many spherical monomers, the trajectories of incoming plasma particles may be blocked by other monomers in the aggregate, and thus the integral over the angles is approximated by numerically computing the LOS factor, LOS_factor $= \iint \cos\alpha d\Omega$ (see Matthews et al. 2012 for a complete description of this treatment). To accomplish this, the surface of the aggregate is divided into many patches, with the resolution on each monomer within an aggregate adjusted for its surface area so that each patch area is approximately equal and the average charge accumulated on each patch is a few electrons. The LOS factor for each patch is determined by finding the open lines of sight from the center of the patch using 1024 test directions. The current density to each patch is then calculated as a function of the electric potential at that patch due to the charge on all of the patches, $\Phi_i = (1/2\pi\varepsilon_0)(q_i/r_i) + \sum_{j \neq i} (1/4\pi\varepsilon_0)(q_j/r_{ij})$, where q_i is the charge on a patch with area $= \pi r_i^2$, and r_{ij} is the distance between the centers of patches i and j. The charge on the aggregate is then found from the total current to the grain (the sum of the current densities to each patch multiplied by the patch areas) multiplied by the time interval Δt. This process is iterated in time until the current to the grain is essentially zero, i.e., the grain charge has reached its equilibrium charge, defined by the charge changing by less than 0.01% over several time steps (where a time step is typically 2% of the estimated equilibrium charging time).

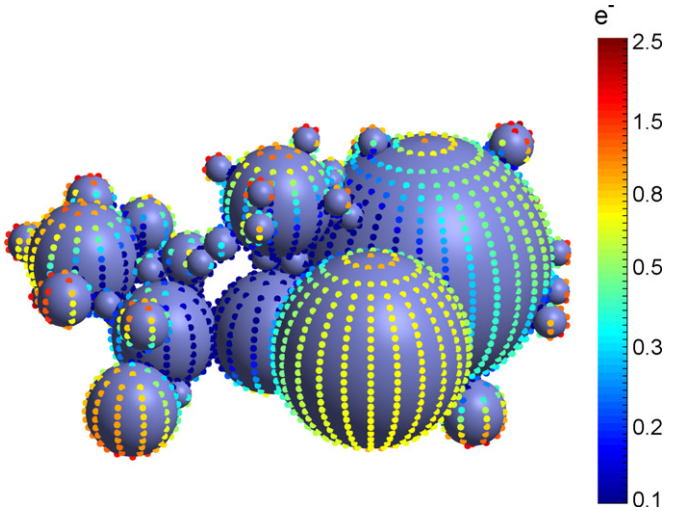

Figure 1. Charge on aggregate. The points indicate the center of each patch, with the number of electrons on each patch indicated by the color bar on the right. The greatest surface charge densities are on the outer extremities of the aggregate.

(A color version of this figure is available in the online journal.)

It should be noted that the assumed straight-line trajectories of the plasma particles are an approximation in determining the blocked orbits to the grain surface. Numerical simulations show that typical plasma particle trajectories that deviate from straight line paths have a radius of curvature at the collision point which is much larger than the aggregate diameter. Thus, over a typical distance between monomers, the approximation of a straight line is fairly good in using the blocked lines of sight to place restrictions on the angle of integration.

The dust grain material modeled in this study is silicates, which is a dielectric. As such, the charge is assumed to remain at the point of contact. While the charge on a grain is expected to redistribute itself to minimize the potential on the surface, the OML_LOS code predicts that the majority of the charge is located at the extremities of the aggregate surface, as shown in Figure 1. For this sample aggregate, the potential at any point

on the surface does not differ from the average surface potential by more than 2%.

2.1 Stochastic Charging

The charge collected on each patch will experience fluctuations since both ions and electrons are attached to the patch at random times. Since the ion and electron currents to each patch as a function of the charges of the patches of the aggregate are known (as described above), the charge fluctuations of the patches can be modeled as follows.

Defining the vector of elementary charges collected on the patches $\mathbf{Z} = \{Z_1, Z_2, \ldots, Z_M\} \in \mathbb{R}^M$, where M is the total number of patches on the aggregate (e.g., Z_2 is the number of elementary charges collected on the patch number 2), and $P(\mathbf{Z}, t)$ as the probability density function of a state at which patch number 1 has Z_1 charges, patch number 2 has Z_2 charges, etc., and assuming that $\mathbf{Z}$ undergoes a Markov process (Van Kampen 2007), a master equation can be developed as follows:

$$\frac{dP(\mathbf{Z}, t)}{dt} = \sum_{p=1}^{M} I_{i,p}(\mathbf{Z} - \mathbf{e}_p)P(\mathbf{Z} - \mathbf{e}_p, t) + I_{e,p}(\mathbf{Z} + \mathbf{e}_p)P(\mathbf{Z} + \mathbf{e}_p, t) - [I_{i,p}(\mathbf{Z}) + I_{e,p}(\mathbf{Z})]P(\mathbf{Z}, t). \quad (3)$$

In this equation, $I_{i,p}(\mathbf{Z})$ and $I_{e,p}(\mathbf{Z})$ are the electron and ion currents, respectively, to patch number p, and $\mathbf{e}_j \in \mathbb{R}^M$ is the unit vector, e.g., $\mathbf{e}_3 = \{0, 0, 1, \ldots, 0\}$. Equation (3) is a generalized form of the master equation given by Matsoukas & Russell (1995) and Shotorban (2011) and is formulated to determine the charge collected on the entire surface of the grain, utilizing the total ion and electron currents to the grain. As such, Equation (3) may be regarded as a gain-loss equation for the probabilities of the separate charge states of the patches, where it is assumed that no charge is transferred from one patch to another.

Using a Kramers–Moyal expansion (Gardiner 2004), a Fokker–Planck equation may be obtained from the master Equation (3)

$$\frac{\partial P(\mathbf{Z}, t)}{\partial t} = \sum_{p=1}^{M} \frac{\partial}{\partial Z_p}[I_{e,p}(\mathbf{Z}) - I_{i,p}(\mathbf{Z})]P(\mathbf{Z}, t) + \frac{1}{2}\frac{\partial^2}{\partial Z_p^2}[I_{e,p}(\mathbf{Z}) + I_{i,p}(\mathbf{Z})]P(\mathbf{Z}, t). \quad (4)$$

It can be shown (Gardiner 2004) that this equation is statistically equivalent to the following stochastic differential equation (SDE) for the charge of each patch:

$$dZ_p(t) = [I_{i,p}(\mathbf{Z}(t)) - I_{e,p}(\mathbf{Z}(t))]t + \sqrt{I_{e,p}(\mathbf{Z}(t)) + I_{i,p}(\mathbf{Z}(t))}dW_p(t), \quad (5)$$

where $Z_p(t)$ is the time-dependent charge of patch p, $\mathbf{Z}(t)$ is the time dependent charge of the vector of patch charges, and $W_p(t)$ is a Weiner process. Equation (5), without the last term on the right-hand side, represents the change in the charge of the patch when random charge fluctuations are neglected. The SDEs can be solved numerically using the Euler–Maruyama method (Gardiner 2004):

$$Z_p^{(n+1)} = Z_p^{(n)} + [I_{i,p}(\mathbf{Z}^{(n)}) - I_{e,p}(\mathbf{Z}^{(n)})]\Delta t + \sqrt{I_{e,p}(\mathbf{Z}^{(n)}) + I_{i,p}(\mathbf{Z}^{(n)})}\sqrt{\Delta t}\xi_p, \quad (6)$$

where Δt is the time step, $Z_p^{(n)}$ is the charge of patch number p at time step n, and ξ_p is a random number with a normal distribution.

There has been also a theoretical work on the mean and variance of the global charge collected on the surface of a spherical grain at the stationary states. For Maxwellian electron and ion distributions with equal electron and ion temperature, $T_e = T_i$, the mean charge on a grain is given by (Matsoukas and Russell 1995)

$$Z = C\frac{4\pi\varepsilon_0 akT_e}{e^2}\ln\frac{n_i}{n_e}\left(\frac{m_e}{m_i}\right)^{1/2}, \quad (7)$$

where Z is the average charge number on a grain of radius a and $n_{e,i}$, $m_{e,i}$ are the electron and ion number density and mass. In Equation (7), C is a constant on the order of unity, weakly dependent on T_e/T_i and M_e/M_i. Furthermore, Matsoukas & Russell (1995) show that for equal ion and electron temperature, the variance of the grain global charge distribution is given by

$$\sigma^2 = \frac{1 - Z/\tau}{2 - Z/\tau}\tau, \quad (8)$$

where $\tau = 4\pi\varepsilon_0 akT_e/e^2$.

Calculating the stochastic charging of multiple surface patches as given in Equation (6), the charging history of a single spherical grain with radius $a = 0.5\ \mu$m is shown in Figure 2. (The plasma environment assumed is representative of conditions in a protoplanetary disk, with the electron and ion densities, n_e and n_i, set as discussed below.) As shown, the charge fluctuates about the equilibrium charge (Figure 2(a)) with a normal distribution (Figure 2(b)). As expected, the average charge Z and variance are linearly proportional to the grain radius (Figure 3), though the variance in the grain charge tends to be greater than that predicted by Equation (8), especially for the larger grain charges. This is possibly due to the fact that the analytic solution given in Equation (8) assumes a spherical particle with an isopotential surface, whereas in this case the potential on the surface can vary at each point as the charge fluctuates.

3. AGGREGATION WITH STOCHASTIC CHARGING

Grain coagulation was modeled employing an initial population of silicate spheres having radii from $0.5 \leqslant a \leqslant 10\ \mu$m and a power-law size distribution $n(a)da \propto a^{-3.5}\ da$. Plasma conditions were chosen to be a simple model representative of a possible protoplanetary disk environment, with hydrogen plasma having equal electron and ion temperature, $T_e = T_i = 900$ K. For a dusty plasma, the quasineutrality condition is $Z_e n_e + Z_i n_i + Z_d n_d = 0$, where n_e, n_i, and n_d refer to the electron, ion, and dust densities, respectively, and $Z_{e,i,d}$ is the average charge number of each species. Two different plasma densities were used, one corresponding to low dust densities, so that a negligible percentage of the electrons reside on the dust grains, $n_e = n_i = 5 \times 10^8$ m^{-3}, and one in which the dust density is large enough that the electrons in the plasma are depleted, $n_e = 0.1\ n_i$ (Matthews et al. 2012). In the second case, the dust charge is reduced as compared to the first (see Figure 3). The relative velocities between two interacting dust grains were set assuming that the grains were small enough to be strongly coupled to turbulent eddies in a protoplanetary disk (Ormel and Cuzzi 2007). Thus, the relative velocity between grains is proportional to the difference in their stopping times, $t_s = 3m/4c_g\rho_g\sigma$, where c_g and ρ_g are the sound speed in the surrounding medium and

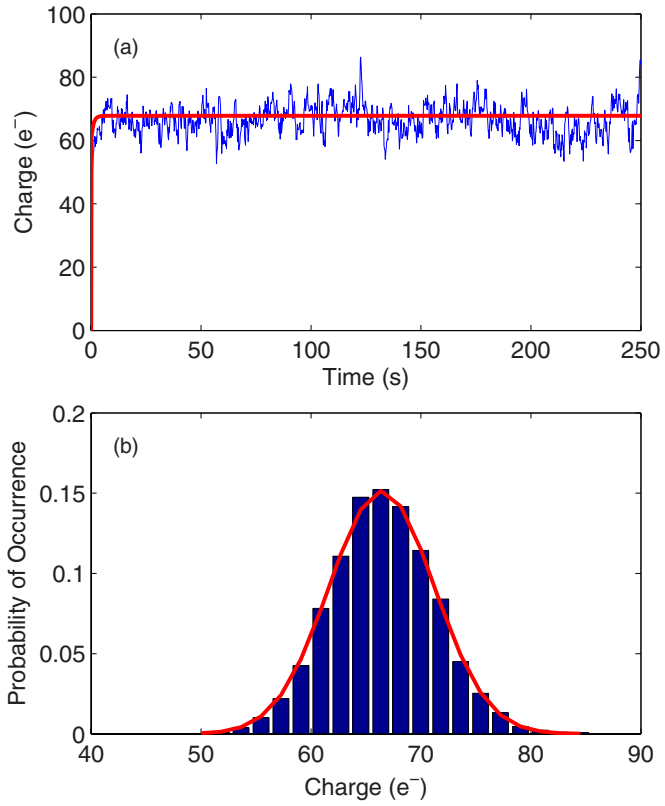

Figure 2. (a) Stochastic charging history of a spherical grain with radius $a = 0.5\ \mu$m for a hydrogen plasma with $n_e = n_i = 5 \times 10^8$ m^{-3} and $T_e = T_i = 900$ K. The charging history of the same grain under the same plasma conditions without the effects of stochastic charging taken into account is shown by the gray (red online) line. (b) Probability distribution of the charge on the grain. The histogram is obtained from the charge at more than 10,000 time steps after the grain has reached its equilibrium charge, where a time step is ∼2% of the equilibrium charging time. The continuous gray line (red online) represents a normal distribution with the mean and variance obtained from simulation.

(A color version of this figure is available in the online journal.)

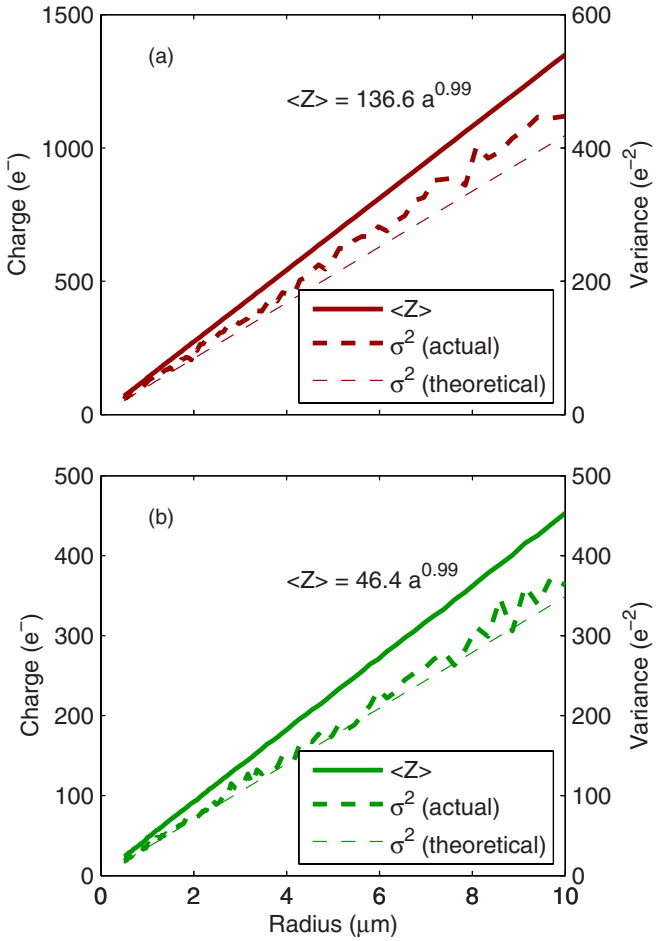

Figure 3. Mean charge collected on a spherical grain (solid line) and the variance (dashed lines) as a function of grain radius. The mean and variance were calculated from 10,000 time steps after a grain had reached its equilibrium charge. The variance in the charge has a linear trend, but tends to be greater than the variance predicted by theory (Equation (8)). Conditions for the hydrogen plasma are (a) $n_e = n_i = 5 \times 10^8$ m^{-3}, (b) $n_e = 0.1\ n_i$.

(A color version of this figure is available in the online journal.)

the mass density of the surrounding medium, respectively, m is the dust particle mass, and σ is its projected cross section, here defined as $\sigma = \pi R_\sigma^2$. For this study, the relative velocities between grains were determined assuming turbulence plus Brownian motion using the conditions described in Matthews et al. (2012). The incoming particle was given a velocity directed toward the center of mass of the target plus an offset with maximum magnitude of $(\sqrt{3}/2)(R_{\sigma 1} + R_{\sigma 2})$.

As the modeled interaction time between two colliding grains is very short compared to the charging time, the charge on each grain was assumed to be constant throughout the interaction process. Using the data shown in Figure 3, incoming monomers were given a charge based on a normal deviation from the mean charge found for stochastic charging. Upon a successful collision, the resulting aggregate was stochastically charged using OML_LOS for a set number of time steps after equilibrium was reached and saved to a library. Thus, the charge on each aggregate was randomly set to some deviation from the average charge.

Typically, growth of porous aggregates is characterized by the types of collisions modeled. In ballistic particle-cluster agglomeration (BPCA), growth proceeds through the addition of single monomers to a cluster, resulting in dense aggregates. In ballistic cluster-cluster aggregation (BCCA), collisions occur between clusters of the same size (number of monomers; Meakin 1991). Quasi-BCCA (QBCCA) growth has also been modeled, in which collisions occur between two clusters with a fixed mass ratio (Okuzumi et al. 2009). In this study, aggregates are created through collisions between an initial polydisperse collection of spherical monomers. The numerical model, Aggregate-Builder, is used to simulate pairwise interactions of colliding particles and includes the accelerations caused by interaction of charged grains as well as rotations induced by off-center collisions and torques caused by the electric dipole interactions (Matthews et al. 2012, 2007; Matthews & Hyde 2009). The position and orientation of each particle are tracked, and a successful collision is detected only when two constituent monomers touch or overlap. A missed collision is recorded when the two particles are receding from each other. As each new aggregate is created, it is saved in a library, and subsequent aggregates are grown through collisions between these aggregates or monomers. In this way, collisions between all possible mass ratios are sampled, with the charge and morphology of each aggregate resolved. The aggregates were built in three generations, with the first generation grown to a size $N = 20$ monomers through BPCA collisions, and the second generation grown to a size $N \sim 200$ through collisions with monomers (60% probability) or first-generation aggregates (40% probability). Third-generation

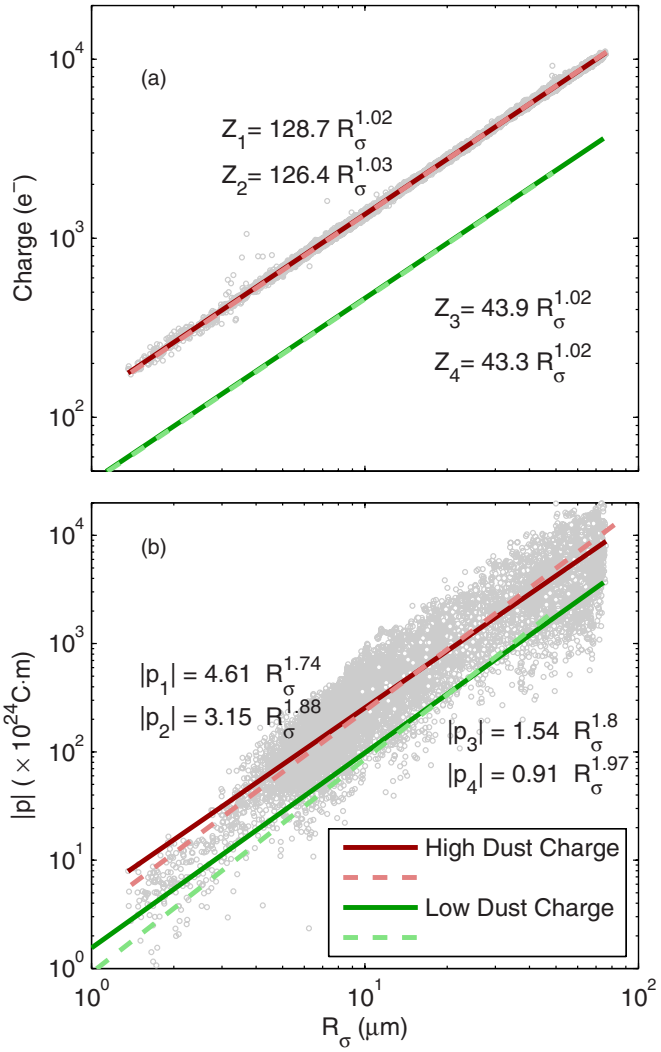

Figure 4. Aggregate charge (a) and dipole moment (b) as a function of the equivalent radius. Lines shown are linear log–log fits to the charge on all of the aggregates. The solid lines indicate the results from stochastic charging, while the dashed lines indicate the results of non-stochastic charging. Data points for ∼12,000 aggregates from the high dust charge, stochastic case are shown to indicate the spread in the data. The subscripts on Q and $|p|$ refer to the charging conditions, with 1, 2 = high dust charge, stochastic/non-stochastic charging, respectively, and 3, 4 = low dust charge, stochastic/non-stochastic charging, respectively.

(A color version of this figure is available in the online journal.)

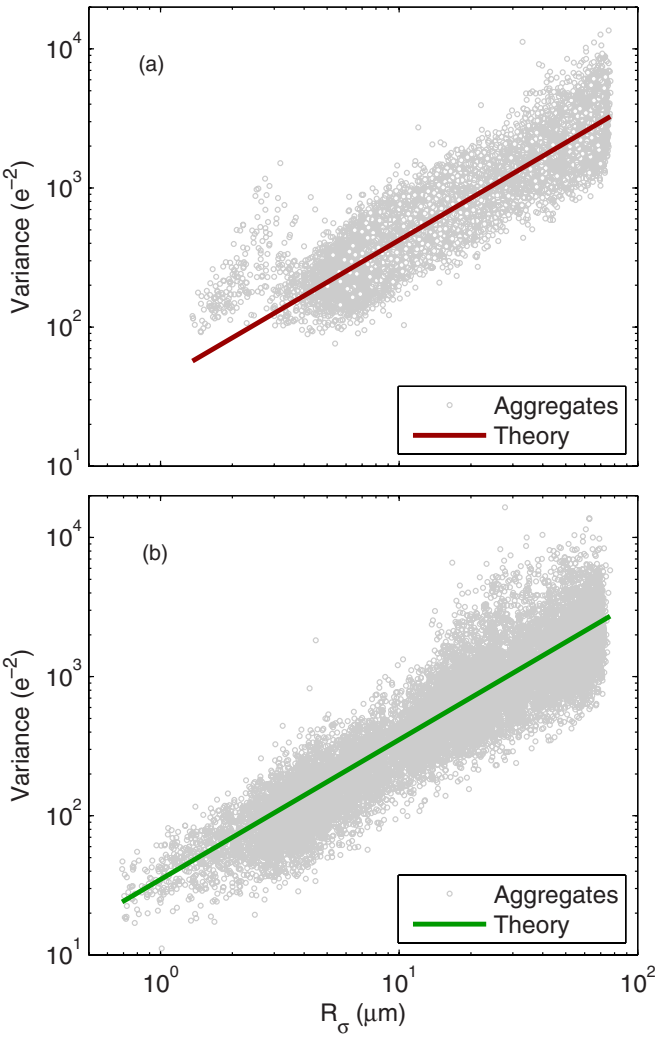

Figure 5. Variance in charge on aggregates for (a) $n_e = n_i$ and (b) $n_e = 0.1\ n_i$. The variance for each aggregate is calculated from the charging history after the aggregate. The line represents the variance as calculated by Equation (8), with $\langle Q \rangle$ given by the equations for the fit lines in Figure 4(a).

(A color version of this figure is available in the online journal.)

aggregates were grown to a size $N \sim 2000$ through collisions with monomers (50%), first-generation aggregates (30%), or second-generation aggregates (20%).

4. AGGREGATION RESULTS

Results for the aggregates produced as described above are shown below. The data are compared for stochastic and non-stochastic charging for the two different plasma conditions (denoted as "high dust charge" for $n_e = n_i$ and "low dust charge" for $n_e = 0.1\ n_i$) and neutral aggregates.

Figure 4 shows the charge on the aggregates as a function of their equivalent radius, R_σ, the average radius of the projected cross section of an aggregate. As expected, only a small difference can be seen in the average aggregate charge when considering charging as a stochastic process (Figure 4(a)). Fit lines for each of the four models (high dust charge/stochastic, high dust charge/non-stochastic, low dust charge/stochastic, and low dust charge/non-stochastic, respectively) exhibit essentially the same slope, which is a result of the LOS factor being closely related to an aggregate's physical characteristics (Ma et al. 2013). The dipole moments on the aggregates are also similar in both charge cases (Figure 4(b)); however, stochastic charging does lead to a difference in the slopes of the fit lines, with the non-stochastically charged dust having a steeper slope. These differences are small compared to the scatter in the data. It should be noted that the non-stochastically charged aggregates with small dust charge did not grow to as large a size; this will be discussed below.

The variance in the charge on the aggregates is shown in Figure 5, with the variance calculated using Equation (8) overlaid for comparison. While this line is a good fit for the average variance, the scatter in the data points is much larger than the scatter in the mean charge (Figure 4), covering more than an order of magnitude. In Figure 5(a), the data points for $R_\sigma < 3\ \mu$m have a variance considerably larger than the mean variance predicted by theory. These points mainly represent $N = 2$ aggregates, and in the highly charged case they consist

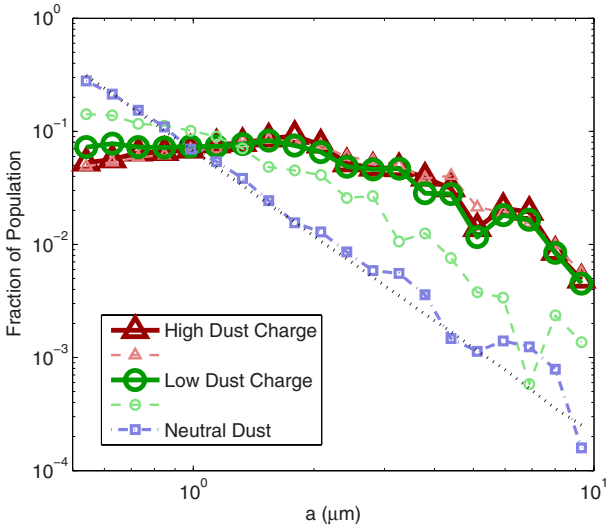

Figure 6. Size distribution of monomers within third-generation aggregates. The area under each curve is normalized to one, with each data point representing the fraction of the total population within a given size bin of logarithmic width Δa. The heavy, darker symbols represent stochastic charging cases, while results for aggregation without stochastic charging are shown by the smaller, lighter symbols. All aggregates were built from an initial population with a power-law distribution, as indicated by the dotted line. The monomers within uncharged aggregates built from this distribution closely follow this trend. Charged aggregates contain a greater proportion of large monomers. While stochastic charging has little effect for the highly charged aggregates, the opposite is true for slightly charged aggregates.

(A color version of this figure is available in the online journal.)

of monomers which have a large difference in radii, unlike the low dust charge case where the $N = 2$ aggregates can consist of monomers of the same radii. Thus, the greater variance is due to the difference in monomer radii and may also reflect the fact that R_σ is not a good defining characteristic for these small aggregates.

The differences between the two charging processes become more apparent when the physical characteristics of the aggregates are examined. Figure 6 shows the monomer distribution within the third-generation aggregates. The initial distribution of monomers is set as a power law with index $\alpha = -3.5$. Charged aggregates have a larger number of large monomers incorporated into the aggregates than do aggregates built from uncharged dust, with this number increasing as the grain charge increases. This is a result of the large relative velocities needed in order to overcome the coulomb repulsion barrier, with turbulent relative velocities depending on the differences in the grain radii. For the highly charged dust (plasma densities $n_e = n_i$), stochastic charging causes very little difference in this distribution. However, for the less highly charged dust (plasma densities $n_e = 0.1\ n_i$), stochastic charging flattens the monomer distribution within the aggregates, similar to the highly charged populations.

This has an effect on the physical characteristics of the aggregates, as well, as shown in Figure 7. More highly charged dust results in aggregates with greater mass (Figure 7(a)), a larger equivalent radius (Figure 7(b)), and a smaller compactness factor (Figure 7(c)) for a given number of monomers contained within the aggregate (N). The greater aggregate mass for a given number of monomers is directly related to the distribution of monomers within the aggregates. Thus, aggregates in the two populations of highly charged aggregates and the stochastically charged population of dust with low charges have similar

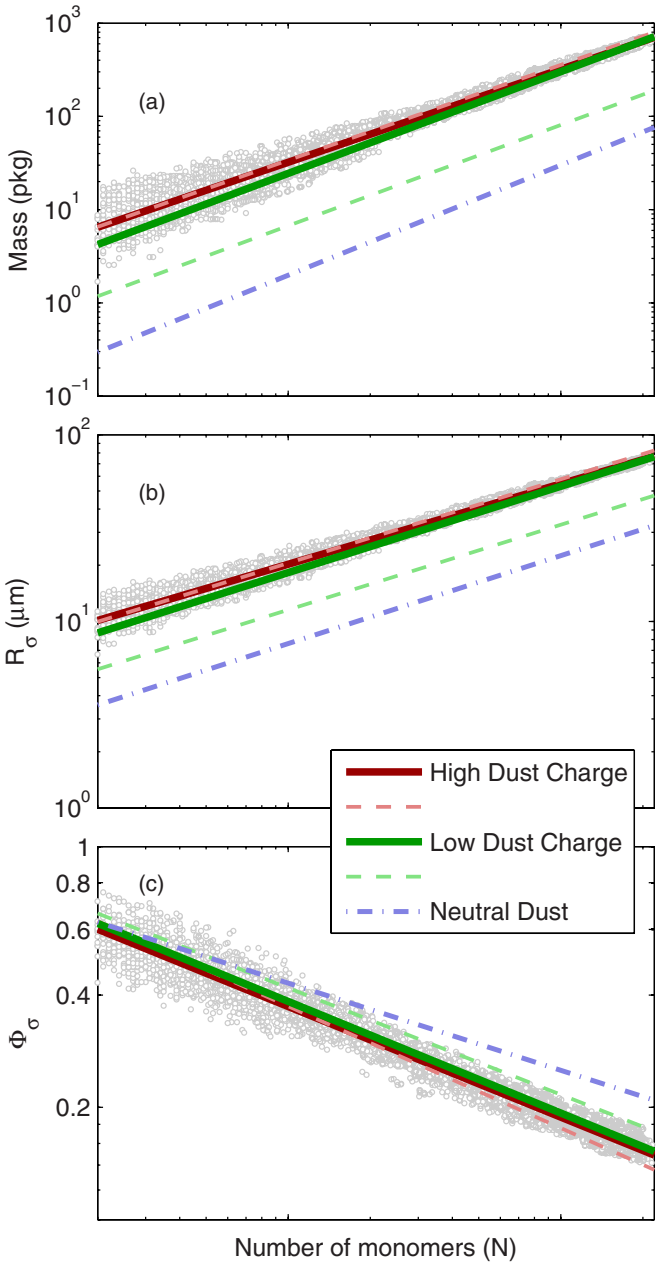

Figure 7. Mass (a), equivalent radius (b), and compactness factor (c) as a function of the number of monomers in an aggregate. Data points shown for the high dust charge/stochastic charging case. Lines represent linear log–log fits to each of the models, with the solid lines indicating stochastic charging and the dashed lines indicating the non-stochastic charging cases.

(A color version of this figure is available in the online journal.)

masses. Stochastic charging effects also cause the aggregates in the low dust charge population to have larger effective radii and lower compactness factors, similar to the more highly charged aggregates. It is interesting to note that at large aggregate sizes, aggregates in both of the stochastically charged cases have very similar compactness factors, slightly more compact than the highly charged case, and slightly less compact than the low dust charge case. A probability density estimate of the compactness factor for the third-generation aggregates (Figure 8) shows that the stochastically charged populations not only have similar compactness factors, intermediate to the two non-stochastic charging cases, but are more sharply peaked about the most probable value than the non-stochastically charged populations, as

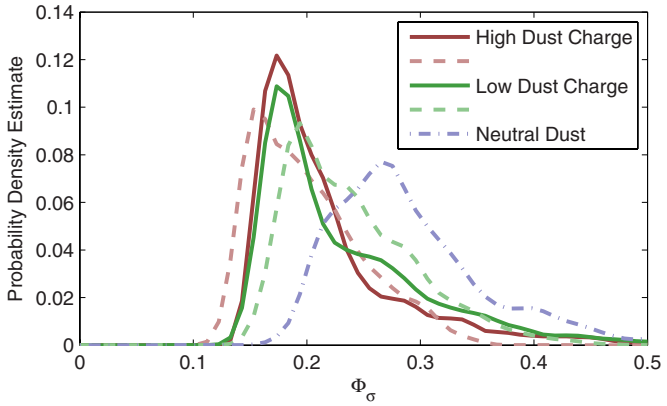

Figure 8. Probability density estimate of the compactness factor for the third-generation aggregates. The solid lines indicate stochastic charging, and the dashed lines indicate the non-stochastic charging cases.

(A color version of this figure is available in the online journal.)

well. The physical differences are easily seen in three sample aggregates shown for the low-charge non-stochastic, high-charge stochastic, and high-charge non-stochastic cases in Figure 9. Each of the aggregates has approximately 2000 monomers and is drawn on the same scale. The low-charge non-stochastic aggregate (Figure 9(a)) is much smaller in size and contains many tiny monomers, resulting in the most compact configuration. The high-charge non-stochastic aggregate (Figure 9(c)) is much more open with a lower compactness factor, even though it has essentially the same distribution of monomer sizes as the high-charge, stochastically charged aggregate (Figure 9(b)), which is similar in radial extent and fluffiness to the largest aggregates in the low-charge, stochastic case.

Thus, while stochastic charging does not have much effect on the distribution of monomers which are incorporated into the highly charged aggregates (which determines the aggregate mass), it does affect the aggregate morphology, which will affect how well the grain is coupled to the gas environment and the turbulence-driven relative velocities, in turn affecting the collision rates.

Figure 10 shows the collision probability, defined as the ratio of the number of successful collisions to the sum of the successful and missed collisions (all calculated particle interactions), as a function of the target aggregate size (the number of monomers within an aggregate). The neutral particles have a collision probability less than one due to the collision offset and the irregular structure of the aggregates; as an aggregate grows larger in size, an incoming particle is more likely to pass through the empty space between the aggregate's "arms". Charged particles, as expected, have low collision probabilities which increase as the target grows in size, thus allowing for the target and incoming particle to have a greater relative velocity. As shown, stochastic charging has little effect on the collision probability for the first-generation aggregates, where aggregates grow by the addition of a single monomer. However, there is a significant difference in the collision probability for second- and third-generation aggregates. Stochastic charging increases the collision probability in the second and third generations for the highly charged dust, but decreases the collision probability for the low dust charge case. The cause of this is found by examining the types of particles which are successfully incorporated into a larger aggregate.

Figure 11 shows the average size (number of monomers) of the incoming particle successfully integrated into larger aggregates, as a function of the resulting aggregate size. Stochastically

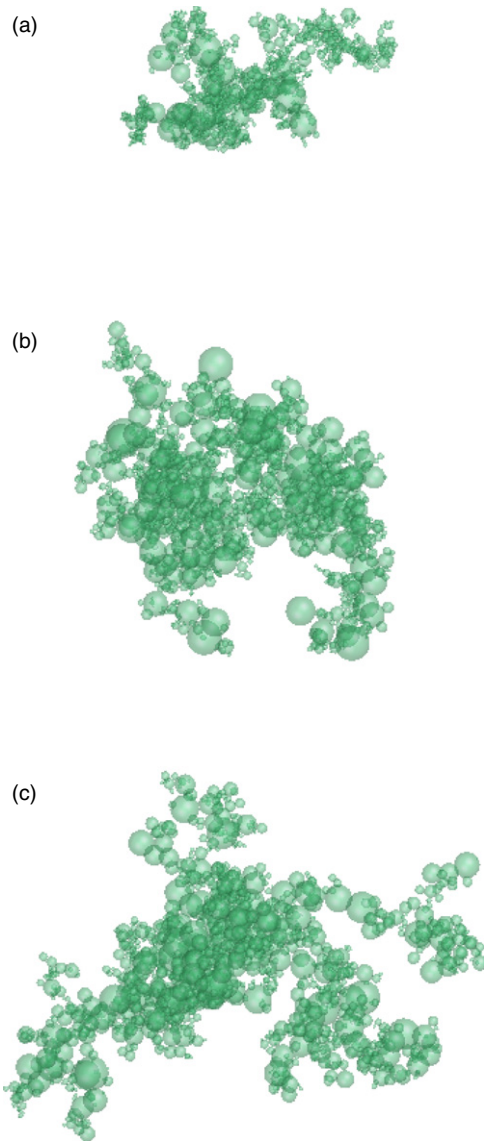

Figure 9. Representative aggregates built with (a) low dust charge, non-stochastic charging, $N = 2015$, $R_\sigma = 44.4$ μm, $\Phi_\sigma = 0.176$; (b) high dust charge, stochastic charging, $N = 2031$, $R_\sigma = 74.7$ μm, $\Phi_\sigma = 0.157$; and (c) high dust charge, non-stochastic charging, $N = 2006$, $R_\sigma = 81.2$ μm, $\Phi_\sigma = 0.133$. The aggregates were chosen to most closely match the average compactness factor for each case.

(A color version of this figure is available in the online journal.)

charged dust incorporated larger incoming particles into the second-generation aggregates as compared to the corresponding non-stochastically charged cases. This appears to be due to the fact that stochastically charged dust aggregates were less likely to successfully collide with monomers (Figure 12(a)). The opposite trend is seen for third-generation aggregates, however, with the size of an added aggregate trending toward a constant size. By examining the type of successful collisions for the third-generation aggregates (Figure 12(b)), it can be seen that the stochastically charged dust grains were more likely to incorporate first-generation aggregates, but less likely to incorporate second-generation aggregates. Thus, the aggregates that were swept up tend to be of a similar size regardless of the size of the target aggregate. In addition, it can be seen that for the stochastically charged dust, the highly charged grains were slightly more

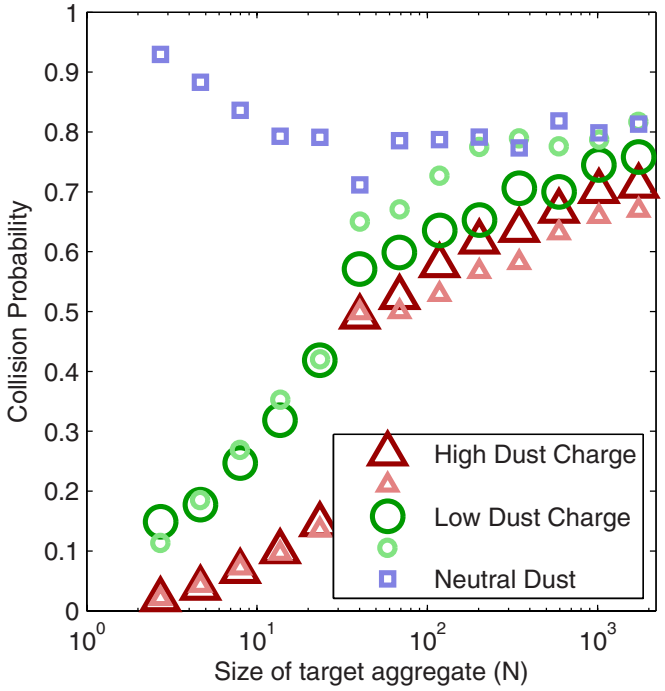

Figure 10. Collision probability as a function of number of monomers within the target aggregate. The smaller, lighter symbols indicate cases with non-stochastic charging. Collision probabilities are strongly affected by the type of collisions: first-generation aggregates ($N \leqslant 20$) only have collisions between single spherical monomers and a target aggregate, while second-generation ($20 < N \leqslant 200$) and third-generation ($200 < N \leqslant 2000$) aggregates have collisions between both individual monomers and smaller aggregates.

(A color version of this figure is available in the online journal.)

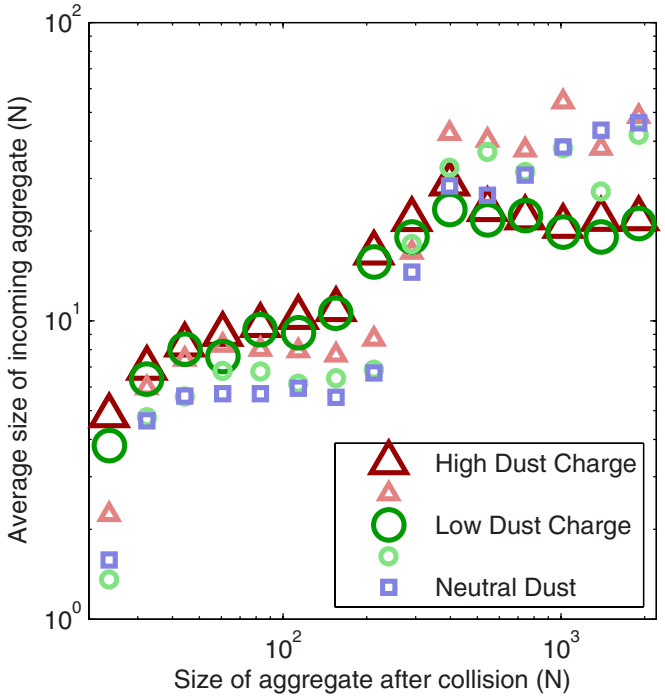

Figure 11. Average size of incoming grain successfully incorporated into an aggregate. Results are shown only for second- and third-generation aggregates, with the data for non-stochastic charging indicated by the smaller, lighter symbols.

(A color version of this figure is available in the online journal.)

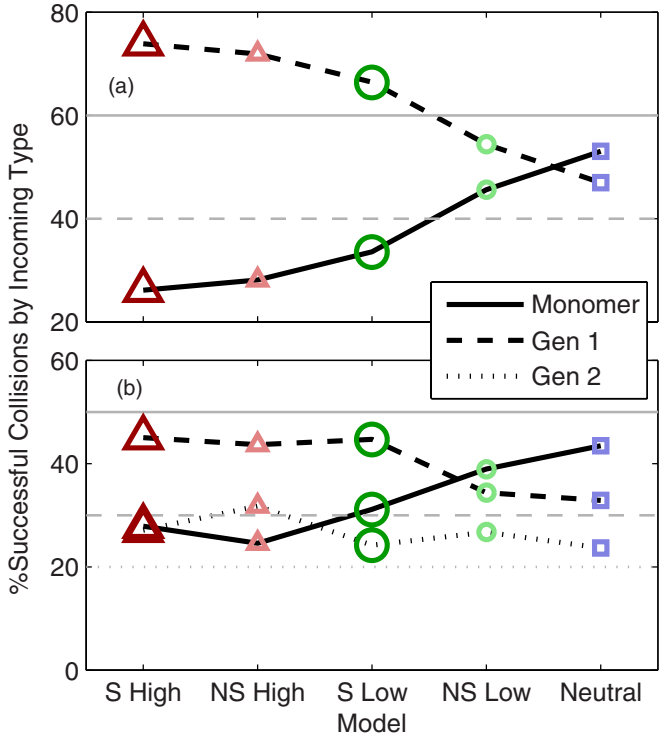

Figure 12. Percentage of successful collisions (out of all successful collisions) by incoming particle type for (a) second-generation aggregates and (b) third-generation aggregates. Light gray lines indicate target percentages for the incoming particles: second-generation aggregates are built by selecting an incoming monomer 60% of the time and an incoming aggregate 40% of the time, while third-generation aggregates are built by selecting a monomer 50% of the time, a first-generation aggregate 30% of the time, and a second-generation aggregate 20% of the time.

(A color version of this figure is available in the online journal.)

likely to incorporate monomers, while the low-charge grains were less likely to incorporate monomers.

5. CONCLUSION AND DISCUSSION

The aggregation of charged dust particles was modeled including the effects of stochastic charging fluctuations. Two different dusty plasma environments were modeled, with the dust grains in the first case having larger charges than grains in the second case. As expected, it was observed that stochastic charging effects were greatest for grains having very small charge.

In the case of more highly charged dust, stochastic charging had a very small effect on the physical characteristics of the dust aggregates formed. This behavior was expected since the charge fluctuations are less critical for dust grains with larger charge. The monomer distribution contained within aggregates (Figure 6), mass, and equivalent radius of the aggregates (Figures 7(a) and (b)) were shown to be identical (within the variance of the data) to those found for non-stochastic charging. In this case, stochastically charged aggregates had slightly greater compactness factors (Figure 7(c)). For dust with smaller charge, stochastic charging had a significant effect on the aggregation, although the average charge and dipole moment remained relatively unchanged (Figure 4). The overall characteristics of stochastically charged aggregates tended to match those that of aggregates formed from highly charged dust grains, containing more of the largest monomers from the initial population (Figure 6), and exhibiting larger aggregate radii,

heavier aggregate masses, and fluffier structures for a given number of monomers (Figure 7). It is interesting to note that stochastically charged dust in both cases tended to have the same average compactness factor for the largest aggregates, and the distribution of compactness factors is more sharply peaked than that for non-stochastically charged dust (Figure 8).

Stochastic charging of grains had mixed effects on probability of collisions between grains for the largest, third-generation aggregates (Figure 10). Stochastic charging increased the collision probability for the highly charged dust, but decreased the collision probability for the dust with small charges. As the stochastically charged aggregates grow to greater numbers of constituent monomers, the average size of an aggregate incorporated into a larger one also tends to approach a constant size (Figure 11), while the average size for the non-stochastically charged aggregates continues to increase. The small ($N \leqslant 20$) aggregates tend to be more efficient at colliding with the larger grains than the monomers (Figure 12). This is likely due to the fact that the large, fluffy aggregates and small, compact aggregates formed through BPCA collisions have the greatest relative velocities and thus the greatest probability of colliding. In addition, it can be seen that for the stochastically charged dust, the highly charged grains were slightly more likely to incorporate monomers, making the resultant structure more compact (high compactness factor). In contrast, the stochastic fluctuations are more important for the low-charge case. Given that the stochastic charge fluctuations make it just as likely for a grain's charge to be greater than the equilibrium charge as to be less than the equilibrium charge, a larger proportion of the monomer population will have charges great enough to prevent a successful collision. This means that the aggregates in the low-charge dust population are less likely to incorporate monomers; the higher percentage of collisions with small aggregates makes the resultant structure fluffier.

In conclusion, stochastic charging will have the greatest effect in environments where dust charge is very low—typically less than a few hundred elementary charges on monomers ranging in size from 0.5 μm to 10 μm. For this case, the physical characteristics of the resultant aggregates will be similar to those for aggregates built from more highly charged dust. Although these results were obtained for a specific set of plasma conditions, the results should be correct in general in any dusty plasma environment where the dust is expected to have a fairly small charge. Thus, the effects of charged grains on aggregation may extend to greater portions of a protoplanetary disk, to regions where the charge on grains was assumed to have negligible effects on aggregation.

Given that the collision probabilities strongly depend on the relative velocities and thus the compactness parameter of the aggregates, an *N*-body simulation is needed to see how a local dust population evolves, especially as the largest monomers are depleted from the initial population. It would also be of interest to add gas drag representative of turbulent flows to more precisely model the relative velocities between grains and grain rotations caused by gas flow. This is the subject of current research. A detailed examination of the collision statistics will also provide parameters necessary for using a Smoluchowski method, as a statistical approach is needed to model the evolution of a full protoplanetary disk including the effect on ionization and turbulence.

This work was supported by the National Science Foundation under Grant No. 0847127 and by the 2012 Junior Faculty Distinguished Research award provided by the University of Alabama in Huntsville.

REFERENCES

Andrews, S. M., & Williams, J. P. 2005, ApJ, 631, 1134
Balbus, S., & Hawley, J. 1991, ApJ, 376, 214
Blum, J., & Wurm, G. 2008, ARA&A, 46, 21
Cui, C., & Goree, J. 1994, ITPS, 22, 151
Dominik, C., Blum, J., Cuzzi, J., & Wurm, G. 2007, in Protostars and Planets V, ed. B. Reipurth, D. Jewitt, & K. Keil (Tucson, AZ: Univ. of Arizona Press)
Dominik, C., & Tielens, A. G. G. M. 1997, ApJ, 480, 647
Gardiner, C. W. 2004, A Handbook for the Natural and Social Sciences (New York: Springer)
Ivlev, A. V., Morfill, G. E., & Konopka, U. 2002, PhRvL, 89, 195502
Khrapak, S. A., Nefedov, A. P., Petrov, O. F., & Vaulina, O. S. 1999, PhRvE, 59, 6017
Konopka, U., Mokler, F., Ivlev, A. V., et al. 2005, NJPh, 7, 227
Laframboise, J. G., & Parker, L. W. 1973, PhFl, 16, 629
Lapenta, G. 1998, PhyS, 57, 476
Ma, Q., Matthews, L. S., Land, V., & Hyde, T. W. 2013, ApJ, 763, 77
Matsoukas, T., & Russell, M. 1995, JAP, 77, 4285
Matsoukas, T., & Russell, M. 1997, PhRvE, 55, 991
Matthews, L. S., Hayes, R. L., Freed, M. S., & Hyde, T. W. 2007, ITPS, 35, 260
Matthews, L. S., & Hyde, T. W. 2004, ITPS, 32, 586
Matthews, L. S., & Hyde, T. W. 2008, ITPS, 36, 310
Matthews, L. S., & Hyde, T. W. 2009, NJPh, 11, 063030
Matthews, L. S., Land, V., & Hyde, T. W. 2012, ApJ, 744, 8
Meakin, P. 1991, RvGeo, 29, 317
Okuzumi, S. 2009, ApJ, 698, 1122
Okuzumi, S., Tanaka, H., & Sakagami, M. 2009, ApJ, 707, 1247
Okuzumi, S., Tanaka, H., Takeuchi, T., & Sakagami, M. 2011a, ApJ, 731, 95
Okuzumi, S., Tanaka, H., Takeuchi, T., & Sakagami, M. 2011b, ApJ, 731, 96
Ormel, C. W., & Cuzzi, J. N. 2007, A&A, 466, 413
Paszun, D., & Dominik, C. 2009, A&A, 507, 1023
Sano, T., Miyama, S. M., Toyoharu, U., & Nakano, T. 2000, ApJ, 543, 486
Shotorban, B. 2011, PhRvE, 83, 066403
Shotorban, B. 2012, PhPl, 19, 053702
Simpson, I. C. 1978, Ap&SS, 57, 381
Suyama, T., Wada, K., & Tanaka, H. 2008, ApJ, 684, 1310
Van Kampen, N. G. 2007, Stochastic Processes in Physics and Chemistry (Amsterdam: Elsevier)
Whipple, E. C. 1981, RPPh, 44, 1197